



**HAL**  
open science

## **Accessory mineral constraints on crustal evolution : elemental fingerprints for magma discrimination**

Emilie Bruand, Mike Fowler, Craig Storey, Oscar Laurent, Clementine  
Antoine, Martin Guitreau, Esa Heilimo, Oliver Nebel

### ► **To cite this version:**

Emilie Bruand, Mike Fowler, Craig Storey, Oscar Laurent, Clementine Antoine, et al.. Accessory mineral constraints on crustal evolution : elemental fingerprints for magma discrimination. *Geochemical Perspectives Letters*, In press. hal-02462901v1

**HAL Id: hal-02462901**

**<https://hal.science/hal-02462901v1>**

Submitted on 31 Jan 2020 (v1), last revised 11 Mar 2020 (v2)

**HAL** is a multi-disciplinary open access archive for the deposit and dissemination of scientific research documents, whether they are published or not. The documents may come from teaching and research institutions in France or abroad, or from public or private research centers.

L'archive ouverte pluridisciplinaire **HAL**, est destinée au dépôt et à la diffusion de documents scientifiques de niveau recherche, publiés ou non, émanant des établissements d'enseignement et de recherche français ou étrangers, des laboratoires publics ou privés.

1 **Accessory mineral constraints on crustal evolution : elemental fingerprints for magma**  
2 **discrimination**

3  
4 Bruand Emilie, Fowler Mike, Storey Craig, Laurent Oscar, Antoine Clementine, Guitreau  
5 Martin, Heilimo Esa, Nebel Oliver

6  
7  
8 Abstract

9 Underexplored accessory minerals such as titanite and apatite have the potential to give  
10 insights into the nature and the petrogenesis of their host rock. Their trace element and REE-  
11 rich compositions carry a record of crystallisation history and chemical characteristics of their  
12 source. Moreover, titanite and, to a certain extent, apatite are resistant to erosion during  
13 sedimentary cycles which makes them ideal to reconstruct the history of long-eroded  
14 continental landmasses. Here we report new trace element data on apatite and titanite from  
15 granitoids of different Archean cratons and comparative granitoids from the Phanerozoic.  
16 Trace element signatures of both minerals reveal systematic chemical trends in Y, LREE and  
17 Sr contents related to the nature of their host magma, which are used to construct  
18 discrimination diagrams delineating Archean TTGs from sanukitoids, and modern adakites  
19 from S/I-type granites. By comparing Archean granitoids (TTG and sanukitoids) and their  
20 Phanerozoic counterparts (adakite and high Ba-Sr granites), we show that the robust nature  
21 of these phases makes them reliable recorders of petrogenetic information from Archean  
22 rocks, that usually have been affected by secondary processes (metamorphism, deformation,  
23 hydrothermal activity). Applied to the rock record, both phases potentially provide detailed  
24 archives of magmatic evolution through time.

25

26 1. Introduction

27

28 Rare earth element (REE) bearing minerals have been used widely to date geological events  
29 and are prime archives for magmatic petrogenesis. Their ability to incorporate a range of  
30 trace elements in addition to REE make them extremely useful to track geological processes.  
31 While most studies on accessory minerals have focussed on zircon (e.g. U-Pb, Hf isotopes,  
32 O isotopes, trace elements), the development of more advanced *in-situ* techniques has also  
33 facilitated other phases to be dated (e.g., monazite, Kohn and Vervoort 2008, titanite, Storey  
34 et al. 2007), thus providing additional chronological constraints on host rock history.  
35 However, despite the impressive number of studies on accessory minerals available today  
36 (see Nasdala et al. 2017), knowledge of the behaviour of trace elements within accessory  
37 minerals in rocks that make up the continental crust is still limited. The few contributions

38 focussing on less-studied REE-bearing minerals (e.g. apatite and titanite ; Belousova et al.  
39 2001; Chu et al. 2009; Bruand et al. 2014) have shown that trace element concentrations  
40 retain considerable information relevant to petrogenesis and provenance, potentially even  
41 more than zircon, whose compositional variability in the most common continental igneous  
42 rocks (e.g. granitoids, Grimes et al. 2015) is relatively limited. In experimental work focussing  
43 on metaluminous compositions, Protwake and Klemme (2005, 2006) have suggested that  
44 REE and other trace elements are sensitive to melt evolution. Recent publications based on  
45 a small number of samples (Bruand et al. 2016, 2017, 2019) have shown that apatite and  
46 titanite trace element chemistry combined with O isotopes are useful tracers of granitoid  
47 petrogenesis and therefore have the potential to discriminate the different magmas through  
48 time and could provide an opportunity to track the secular evolution of the early Earth and the  
49 onset of modern-style plate tectonics. For this contribution, we have studied the chemical  
50 signatures of accessory minerals in a range of crust-forming granitoids through time, from a  
51 relatively hot Archaean Earth producing «tonalites-trondjhemites-granodiorites» (TTG)  
52 toward a cooler modern Earth producing plutonic equivalents of the calc-alkaline series  
53 (basalt-andesite-dacite-rhyolite – BADR), via the Neoarchaeon – Palaeoproterozoic transition  
54 to modern plate tectonics signalled by sanukitoids and related rocks. We demonstrate that  
55 their trace element signatures can be used to discriminate between critical magma types and  
56 can be robust with respect to metamorphism. We then discuss the causes of consistent  
57 differences in accessory mineral chemistry and implications of their robust discrimination for  
58 studies of magmatic and crustal evolution through geological times.

59

## 60 2. Granitoid samples and their crustal evolution context

61

62 The granitoid record (Fig. 1) has evolved from the Archean to the Phanerozoic, as a  
63 reflection of Earth's cooling and evolution of tectono-magmatic processes (see Moyen and  
64 Laurent 2018 and references therein). Granitoids representing newly formed continental  
65 crust have hence changed from Archean TTGs, formed by partial melting of mafic crust, via  
66 sanukitoids and related rocks in the Neoarchean and Palaeoproterozoic that carry the  
67 signature of a nascent mantle wedge, towards granodiorites and granites with arc magma  
68 compositions (the plutonic equivalents of BADR). Many fundamental questions remain  
69 regarding the geodynamics of the early Earth, the growth of the continental crust and the  
70 transition to subduction-driven tectonics, some of which may be addressed with a more  
71 complete understanding of timings and proportions of granitoid magma genesis. Here we  
72 present new geochemical data on titanite and apatite from granitoids selected from this  
73 overall temporal progression (i) Archean TTG from three different cratons (Slave Province,  
74 Karelia and Kaapvaal), (ii) sanukitoids from the Karelia and Kaapvaal cratons, (iii)

75 Neoproterozoic calc-alkaline granitoids from Guernsey (UK Channel Islands) in the  
76 Armorican terrane. Studied Archean localities have been affected by metamorphic conditions  
77 up to amphibolite facies. In addition to these, we have included likely Phanerozoic  
78 equivalents to test the impact of metamorphism on their older counterparts: TTG-like  
79 (adakites from Antarctica; Pankhrust et al. 1998) and sanukitoid-like rocks (high Ba-Sr  
80 granites from Caledonian Scotland; Fowler and Rollinson 2012). Detailed sample  
81 descriptions, geological settings and whole-rock compositions can be found in  
82 Supplementary Information.

83

### 84 3. Results

85

86 Trace elements concentrations obtained by LA-ICPMS on single minerals and related  
87 analytical protocols are described in Supplementary Information. After initial data  
88 interrogation using principal component analysis (PCA) on both apatite and titanite datasets,  
89 REEs, Y and Sr were found to be most effective for discriminating magma type. These  
90 results are presented and discussed below.

91

#### 92 3.1. Apatite chemistry

93

94 Chondrite-normalized REE patterns for apatite from all studied samples are plotted on Figure  
95 2A-E. TTG samples (Fig. 2A) are characterized by a systematic depletion in light REE  
96 (LREE) relative to heavy REE (HREE ;  $La_N/Lu_N < 1$ ) usually with a strong negative Eu  
97 anomaly (usually  $Eu/Eu^* = 0.15-0.8$ ). The most depleted patterns tend to have a less  
98 pronounced to absent Eu anomaly and noticeable middle REE (MREE) fractionation from  
99 HREE. Adakite (TTG-like) apatite crystals (Fig. 2B) have a relatively flat LREE pattern  
100 ( $La_N/Sm_N = 0.5-1.8$ ) with slightly lower HREE ( $La_N/Lu_N = 1.5-4$ ) and a negative Eu anomaly  
101 ( $Eu/Eu^* = 0.3-0.4$ ). Typical BADR REE patterns (Fig. 2C) show higher LREE content with  
102 strong enrichment compared to the HREE ( $La_N/Lu_N > 15$ ), with moderate negative Eu  
103 anomalies ( $Eu/Eu^* \approx 0.5$ ). Similarly, sanukitoids and high Ba-Sr granite REE patterns (Fig. 2  
104 D-E) reveal a general enrichment in LREE relative to HREE ( $La_N/Lu_N = 10-100$ ) usually with  
105 moderate negative Eu anomalies ( $Eu/Eu^* \approx 0.4-0.8$ ). In the high Ba-Sr group, the most mafic  
106 samples often lack Eu anomalies.

107 Following the PCA procedure, a  $10^*Sr-LREE-10^*Y$  discrimination diagram was constructed  
108 (Fig. 3A). Apatite from TTG and TTG-like granitoids are clearly distinguishable from other  
109 granitoid types, defining a distinct cluster towards the  $10^*Y$  corner and having Sr contents  
110 ranging between 150 and 430  $\mu g/g$  (Table S3). On the other hand, sanukitoids, sanukitoid-  
111 like and BADR samples are characterized by higher LREE and Sr contents (up to 1000  $\mu g/g$ )

112 and thus form a separate field towards that baseline. Similarly, a  $La_N/Sm_N$  versus Y diagram  
113 (Fig. 4A) highlights a strong compositional difference. TTG and TTG-like apatite grains are Y  
114 rich (up to approximately 4600  $\mu\text{g/g}$ ) with low La ( $< 300 \mu\text{g/g}$ ), whereas sanukitoid, high Ba-  
115 Sr granite and BADR apatite grains define a field poor in Y ( $< 1000 \mu\text{g/g}$ ) and with La up to  
116 approximately 2800  $\mu\text{g/g}$ .

117

### 118 3.2. Titanite chemistry

119

120 REE patterns of titanite from the studied samples are presented in figure 2F-I, although  
121 titanite is not present in all studied samples (see supplementary information). There are  
122 many similarities with the patterns for apatite (Fig. 2A-E). Titanite grains from one TTG  
123 sample (Fig. 2F) are characterized by pronounced LREE depletion relative to HREE (usually  
124  $La_N/Lu_N < 0.5$ ). In contrast with apatite, the patterns have variable, usually large Eu  
125 anomalies ( $Eu/Eu^* = 0.2-40$ ), generally negative for those with higher total REE, positive for  
126 lower total REE. Titanite from sanukitoids and high Ba-Sr granites (Fig. 2G-H) show strong  
127 enrichment of LREE relative to HREE ( $La_N/Lu_N \approx 3-45$ ), usually with a convex-upward LREE  
128 section and a noticeable negative Eu anomaly. A few sanukitoid titanites in each of the  
129 samples studied have steep downward LREE slopes and/or a positive Eu anomaly (Fig. 2G).  
130 The BADR REE patterns (Fig. 2I) are closely comparable with the high Ba-Sr samples, but  
131 can be separated into two groups that are sample specific. Sample EG-07 titanite crystals  
132 have convex-upward LREE ( $La_N/Sm_N = 0.4-0.9$ ) and a negative Eu anomaly ( $Eu/Eu^* \approx 0.6-$   
133  $0.7$ ) whereas one from sample BD-02 has continually decreasing LREE ( $La_N/Sm_N > 1$ ) with  
134 no Eu anomaly (Fig. 2I, Appendix A.1).

135 Using a similar trivariate diagram to apatite (Fig. 3B, but note the different Sr multiplier  
136 accounting for lower Sr contents in titanite), TTG titanite compositions may be discriminated  
137 from all other samples. Titanite from TTG define an end member with high Y (up to 24000  
138  $\mu\text{g/g}$ ) and low Sr (usually  $< 20 \mu\text{g/g}$ ) and LREE (e.g. usually  $La < 150 \mu\text{g/g}$ ) contents  
139 relative to sanukitoids and BADR samples (Y and La contents are up to 4000  $\mu\text{g/g}$ ; Sr  $> 40$   
140  $\mu\text{g/g}$ ).

141

## 142 4. Discussion

143

144 The temporal evolution of granitoids has been well established (Fig. 1, see also Moyen and  
145 Martin 2012 for review). Most TTGs can be discriminated on the basis of several whole-rock  
146 chemical indicators, the most prevalent of which is stronger HREE depletion (Fig. 2J). The  
147 present study has also shown systematic differences in TTG apatite and TTG titanite  
148 compositions relative to sanukitoids and post-Archean granitoids (Figs 2-3), in particular

149 higher Y and HREE contents with low  $La_N/Sm_N$  ratio (Fig. 2, 4A). Intriguingly, this is  
150 completely opposite to the whole-rock signatures (Fig. 2J). In the following text, we attempt  
151 to rationalise such observations in terms of possible controls on apatite and titanite  
152 chemistry, and in the light of current literature.

153

#### 154 4.1 Effects of metamorphism and/or deformation

155

156 Because Archean rocks may have suffered metamorphism and/or deformation, there is the  
157 obvious possibility that accessory mineral chemistry has been modified and record  
158 metamorphic/hydrothermal rather than igneous processes. The studies available on the  
159 impact of metamorphism and hydrothermalism on apatite and titanite are limited (e.g. Broska  
160 et al. 2007) and often describe lithologies and/or whole rock compositions (metapelites or  
161 orthogneisses) that are very different from our samples (e.g., Bea and Montero 1999; Garber  
162 et al. 2017). Therefore, in order to test the robustness of apatite and titanite magmatic  
163 signatures, we have analysed apatite and titanite from Phanerozoic equivalents of TTG  
164 (adakite, Fig. 2B) and sanukitoid (high Ba-Sr granites, Fig. 2E, H), unaffected by any  
165 metamorphic event. Their chondrite-normalized REE patterns correspond closely to the  
166 Archean equivalents (Fig. 2A, D, G) and overlap the relevant fields on the discrimination  
167 diagrams above (Fig. 3, Fig. 4A).

168 A few TTG apatite patterns show extreme depletion in LREE with no Eu anomaly (Fig  
169 2A). This can be explained petrographically, by the observed association of secondary  
170 allanite and apatite, which form on the expense of primary REE-bearing phases (Fig. S1).  
171 The highly LREE-depleted group in our samples, is therefore interpreted to have formed  
172 under high-grade metamorphic conditions and are characterised by lower  $La_N/Sm_N$  but  
173 retains original HREE signatures.

174

#### 175 4.2 Effects of whole-rock composition

176

177 The systematic chemical differences between the accessory mineral groups studied here,  
178 from different types of granitoid, strongly suggest that bulk rock character exerts strong  
179 control on the trace-element composition of accessory minerals.

180

##### 181 4.2.1 The influence of whole rock $SiO_2$

182

183 Partition coefficient studies have shown that incorporation of REE in apatite and titanite  
184 increases with  $SiO_2$  of the magma (Prowatke and Klemme 2005,2006). TTGs studied herein  
185 vary between 65 wt% and 74 wt%  $SiO_2$ , the other granitoids range between 53 and 77 wt%.

186 Within the former, apatite and titanite total REE contents do not systematically increase with  
187 [SiO<sub>2</sub>] of the melt (Appendix A.1). Furthermore, sanukitoid or BADR samples with similar  
188 SiO<sub>2WR</sub> have apatite and titanite characterised by comparatively higher LREE and lower  
189 HREE. Such systematic differences are therefore not controlled simply by silica content.

190

#### 191 4.2.2 The influence of Alumina Saturation Index (ASI)

192

193 The striking dichotomy in the TTG between LREE depletion in the accessory minerals and  
194 LREE enrichment in whole rocks suggests that another LREE-bearing phase is required for  
195 mass balance. Likely contenders would be allanite and monazite, but since these are also  
196 common in many other granitoid types, this is unlikely to be the sole explanation.

197 Figure 4A includes literature data, and highlights the presence of two distinct groups of  
198 apatite that are strongly dependent on ASI. ASI < 1 samples (metaluminous) correspond to  
199 our sanukitoids-BADR apatites (Group 1), whereas peraluminous samples (ASI >1) have a  
200 comparable chemical signature to TTG apatite grains (low LREE and high HREE-Y, Group  
201 2). This corroborates previous studies on apatite (Harrison and Watson 1984; Pichavant et  
202 al. 1992) and monazite (Montel 1986) solubilities, which suggest that apatite solubility  
203 increases with ASI and (to a lesser extent) with SiO<sub>2</sub> in metaluminous magmas. Conversely,  
204 Montel (1986) has shown that monazite solubility decreases as ASI increases. This is also  
205 consistent with the presence of « remaining » primary monazite surrounded by secondary  
206 allanite and apatite identified on the studied Acasta samples (Supplementary Information). It  
207 should be noted that monazite solubility can also be influenced by other factors (e.g. P  
208 content in the melt, Skora and Blundy 2012). In summary, our dataset demonstrates that in  
209 peraluminous compositions early monazite will strongly partition LREE with the remaining  
210 melt relatively enriched in HREE and Y, which will be incorporated by later apatite and  
211 titanite. These conclusions were also reached in previous work on Phanerozoic granitoids (e.g.  
212 Chu et al. 2009).

213

214 Interestingly, apatites from two metaluminous samples are Y-rich and LREE poor  
215 (Fig. 4A), which is inconsistent with the general trend. These exceptions have the highest  
216 SiO<sub>2</sub> content (>73 wt%), a phenomenon also described by Sha and Chappell (1999). High  
217 melt SiO<sub>2</sub> content increases apatite solubility (Harrison and Watson 1984) and therefore  
218 delays its saturation. Consequently, apatite may grow late, allowing early LREE phases  
219 (monazite and/or allanite) to incorporate most of the LREE.

220

#### 221 4.2.3 Other variables

222

223 We have shown above that aluminosity and consequent timing of mineral saturation is a first  
224 order control on accessory mineral chemistry. However, our TTG apatite compositions have  
225 systematically even lower LREE concentrations than published apatite data for peraluminous  
226 rocks (Fig. 4A) so other variables must also be important. For example, previous authors  
227 have inferred that differences in magmatic apatite composition could be related to magma  
228  $fO_2$  (Sha and Chappell 1999; Belousova et al. 2001). It remains unclear whether this is linked  
229 to the nature of the TTG source (e.g. composition such as high  $Na_2O$  and low REE content  
230 compare to other granitoids,  $fO_2$ , temperature,  $H_2O$ -saturated or undersaturated melting) or is  
231 another effect of co-crystallising accessory phases. Experimental constraints are currently  
232 lacking.

233

#### 234 4.2.4 The significance of Sr

235

236 Previous work (e.g. Halla et al. 2009; Moyen 2011) has distinguished high-pressure TTG,  
237 corresponding to a deep source in equilibrium with garnet and rutile but no plagioclase, from  
238 low-pressure TTG consistent with residual plagioclase. As a direct consequence of residual  
239 mineralogy, HP-TTG have low HREE, Nb and Ta and high Sr whereas LP-TTG show the  
240 opposite signature for comparable bulk compositions (e.g. Moyen and Martin 2012). Previous  
241 authors (Belousova et al. 2001; Jennings et al., 2011; Bruand et al. 2014) have shown a  
242 strong correlation between Sr in apatite and in the corresponding whole-rock. Our data sit on  
243 this previously reported correlation. Accordingly, in our apatite dataset, two TTG and our  
244 adakite samples that have typical HP-TTG signature have systematically higher Sr  
245 concentrations than the others that have LP TTG signature (Fig. 4C). Figure 4C also shows  
246 that the HP-TTG apatite analyses have lower Y (and by analogy, HREE). All these  
247 observations confirm that apatite Sr content can allow discrimination between HP and LP-  
248 TTG. Interestingly, correlation between unusually high Sr content of monazite and HP  
249 conditions has also been previously reported in the Bohemian Massif peraluminous rocks  
250 (Finger and Krenn 2007).

251

#### 252 4.4 Implications for crustal evolution research.

253

254 The preservation of magmatic trace element signatures in apatite and titanite, from  
255 metamorphosed terranes such as those of Archean age, provides a useful method to  
256 reconstruct ancient magmatic history. For example, in this study, we demonstrate that  
257 accessory minerals of late Archean granitoids (sanukitoids) are different from Archean TTGs.  
258 Such differences reflect whole-rock compositions which themselves reflect petrogenetic  
259 processes. Thus, the different petrogeneses of TTGs and sanukitoids (early subduction or

260 « drip tectonics » ; Nebel et al. 2018) are reflected by accessory mineral chemistry.  
261 Therefore detailed investigation of the apatite and titanite mineral chemical archive could  
262 tightly constrain the change in geodynamics at the end of the Archean. Finally, our data  
263 reveal an efficient distinction of parental magma types based on REE-Sr-Y alone which  
264 further encourages application to the detrital mineral record. Voluminous data exist from  
265 zircons, but the results described above promise much closer constraints on parent rock  
266 identity, thus providing vital access to the primary history of eroded terranes and helping to  
267 reconstruct the historical evolution of continental crust from the early Earth to the present  
268 day.

269

### 270 **Acknowledgements**

271 We are grateful to Stuart Kearns and J-L Devidal for microanalytical analyses, to Geoff Long  
272 for amazing technical support. This work was supported by the Natural Environment  
273 Research Council (grant NE/I025573/1) and by the French Government Laboratory of  
274 Excellence initiative n° ANR-10-LABX-0006. This is Laboratory of Excellence ClerVolc  
275 contribution number 387. We deeply thank the editor H. Marschall and two anonymous  
276 reviewers for their input.

277

### 278 **Figure Captions**

279 Fig. 1 Cartoon of continental crust evolution, from TTG (blue) and sanukitoid (pink) in the  
280 Archean towards typical arc magma (green) in Proterozoic and Phanerozoic, plus samples  
281 studied in this contribution.

282 Fig. 2 Chondrite-normalised REE patterns for apatite (A-E) and titanite (F-I). J diagram  
283 represents La/Yb vs Yb values normalized to chondrite for whole rock data, modified after  
284 Moyen and Martin (2012). Green and blue fields correspond to post 2.5 Ga granitoids and  
285 TTG, respectively.

286 Fig. 3 Ternary discrimination diagrams;  $10^*Sr-LREE-10^*Y$  for apatite and  $100^*Sr-LREE-10^*Y$   
287 for titanite.

288 Fig.4 Apatite compositions: A - La vs Y diagram discriminating 2 groups of apatite, B -  
289  $La_N/Sm_N$  vs ASI ( $nAl/((nCa-3.33*nP)+nNa+nK)$ ), discriminating peraluminous from  
290 metaluminous compositions and C - Sr vs Y, discriminating apatite from HP- and LP-TTG  
291 magmas.

292

### 293 **References**

294 Bea F, Montero P (1999) Behavior of accessory phases and redistribution of Zr, REE, Y, Th,  
295 and U during metamorphism and partial melting of metapelites in the lower crust: An  
296 example from the Kinzigite Formation of Ivrea-Verbano, NW Italy. *Geochim Cosmochim*

297 Acta 63:1133–1153.

298 Belousova E, Griffin W, O'Reilly SY, Fisher N (2002) Igneous zircon: trace element  
299 composition as an indicator of source rock type. *Contrib to Mineral Petrol* 143:602–622.

300 Belousova EA, Walters S, Griffin WL, O'Reilly SY (2001) Trace-element signatures of  
301 apatites in granitoids from the Mt Isa Inlier, Northwestern Queensland. *Aust J Earth Sci*  
302 48:603–619.

303 Broska I, Harlov D, Tropper P, Siman P (2007) Formation of magmatic titanite and titanite-  
304 ilmenite phase relations during granite alteration in the Tribe?? Mountains, Western  
305 Carpathians, Slovakia. *Lithos* 95:58–71.

306 Bruand E, Fowler M, Storey C, Darling J (2017) Apatite trace element and isotope  
307 applications to petrogenesis and provenance. *Am Mineral* 102:75-84.

308 Bruand E, Storey C, Fowler M (2016) An apatite for progress: Inclusions in zircon and titanite  
309 constrain petrogenesis and provenance. *Geology* 44:91-94.

310 Bruand E, Storey C, Fowler M (2014) Accessory mineral chemistry of high Ba-Sr granites  
311 from Northern Scotland: Constraints on petrogenesis and records of whole-rock  
312 Signature. *J Petrol* 55:1619-1651.

313 Bruand E, Storey C, Fowler M, Heilimo E (2019) Oxygen isotopes in titanite and apatite , and  
314 their potential for crustal evolution research. *Geochim Cosmochim Acta* 255:144–162.

315 Chu MF, Wang KL, Griffin WL, et al (2009) Apatite composition: Tracing petrogenetic  
316 processes in Transhimalayan granitoids. *J Petrol* 50:1829–1855.

317 Finger F, Krenn E (2007) Three metamorphic monazite generations in a high-pressure rock  
318 from the Bohemian Massif and the potentially important role of apatite in stimulating  
319 polyphase monazite growth along a PT loop. *Lithos* 95:103–115.

320 Fowler M, Rollinson H (2012) Phanerozoic sanukitoids from Caledonian Scotland:  
321 Implications for Archean subduction. *Geology* 40:1079–1082.

322 Garber JM, Hacker BR, Kylander-Clark ARC, Stearns M, Seward G (2017) Controls on Trace  
323 Element Uptake in Metamorphic Titanite : Implications for Petrochronology. *J Petrol*  
324 58:1031–1058.

325 Grimes CB, Wooden JL, Cheadle MJ, John BE (2015) “ Fingerprinting ” tectono - magmatic  
326 provenance using trace elements in igneous zircon. *Contrib to Mineral Petrol* 170:1–26.

327 Halla J, Hunen J Van, Heilimo E, Hölttä P (2009) Geochemical and numerical constraints on  
328 Neoproterozoic plate tectonics. 174:155–162.

329 Harrison TM, Watson EB (1984) The behavior of apatite during crustal anatexis: Equilibrium  
330 and kinetic considerations. *Geochim Cosmochim Acta* 48:1467–1477.

331 Jennings ES, Marschall HR, Hawkesworth CJ, Storey CD (2011) Characterization of magma  
332 from inclusions in zircon: Apatite and biotite work well, feldspar less so. *Geology*  
333 39:863–866.

334 Kohn MJ, Vervoort JD (2008) U-Th-Pb dating of monazite by single-collector ICP-MS: Pitfalls  
335 and potential. *Geochemistry, Geophys Geosystems* 9:1–16.

336 Li H, Hermann J (2017) The effect of fluorine and chlorine on trace element partitioning  
337 between apatite and sediment melt at subduction zone conditions. *Chem Geol* 473:55–  
338 73.

339 Montel JM (1986) Experimental determination of the solubility of Ce-monazite in SiO<sub>2</sub>-Al<sub>2</sub>O<sub>3</sub>-  
340 K<sub>2</sub>O-Na<sub>2</sub>O melts at 800°C, 2kbar, under H<sub>2</sub>O-saturated conditions. *Geology* 14:659–  
341 662.

342 Moyen J (2011) *Lithos* The composite Archaean grey gneisses : Petrological significance,  
343 and evidence for a non-unique tectonic setting for Archaean crustal growth. *Lithos*  
344 123:21–36.

345 Moyen J, Laurent O (2018) *Lithos* Archaean tectonic systems : A view from igneous rocks.  
346 303:99–125.

347 Moyen J, Martin H (2012) Forty years of TTG research. *Lithos* 148:312–336.

348 Nasdala L, Broska I, Harlov DE, Macdonald R (2017) Recent progress in the study of  
349 accessory minerals. *Mineral Petrol* 102:431–433.

350 Nebel O, Capitanio FA, Moyen J, et al (2018) When crust comes of age : on the chemical  
351 evolution of Archaean , felsic continental crust by crustal drip tectonics. *J. of the Royal*  
352 *Soc.*

353 Pankrust RJ, Weaver SD, Bradshaw JD, et al (1998) Geochronology and geochemistry of  
354 pre-Jurassic superterranes in Marie Byrd Land, Antarctica. *J Geophys Res* 103:2529–  
355 2547.

356 Pichavant M, Montel JM, Linda R (1992) Apatite solubility in peraluminous liquids :  
357 Experimental data and an extension of the Harrison-Watson model. *Geochemica*  
358 *Cosmochim Acta* 56:3855–3861.

359 Prowatke S, Klemme S (2005) Rare earth element partitioning between titanite and silicate  
360 melts: Henry's law revisited. *Geochim Cosmochim Acta* 70:4997–5012.

361 Prowatke S, Klemme S (2006) Trace element partitioning between apatite and silicate melts.  
362 *Geochim Cosmochim Acta* 70:4513–4527.

363 Sha L-K, Chappell BW (1999) Apatite chemical composition, determined by electron  
364 microprobe and laser-ablation inductively coupled plasma mass spectrometry, as a  
365 probe into granite petrogenesis. *Geochim Cosmochim Acta* 63:3861–3881.

366 Skora S, Blundy J (2012) Monazite solubility in hydrous silicic melts at high pressure  
367 conditions relevant to subduction zone metamorphism. *Earth Planet Sci Lett* 322:104–  
368 114.

369 Storey CD, Smith MP, Jeffries TE (2007) In situ LA-ICP-MS U–Pb dating of metavolcanics of  
370 Norrbotten, Sweden: Records of extended geological histories in complex titanite



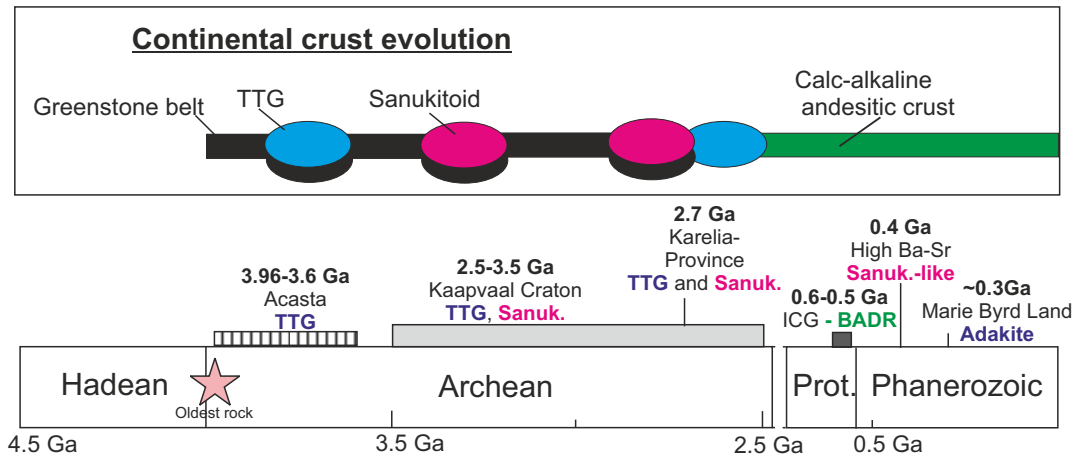


Fig.1 Bruand et al.

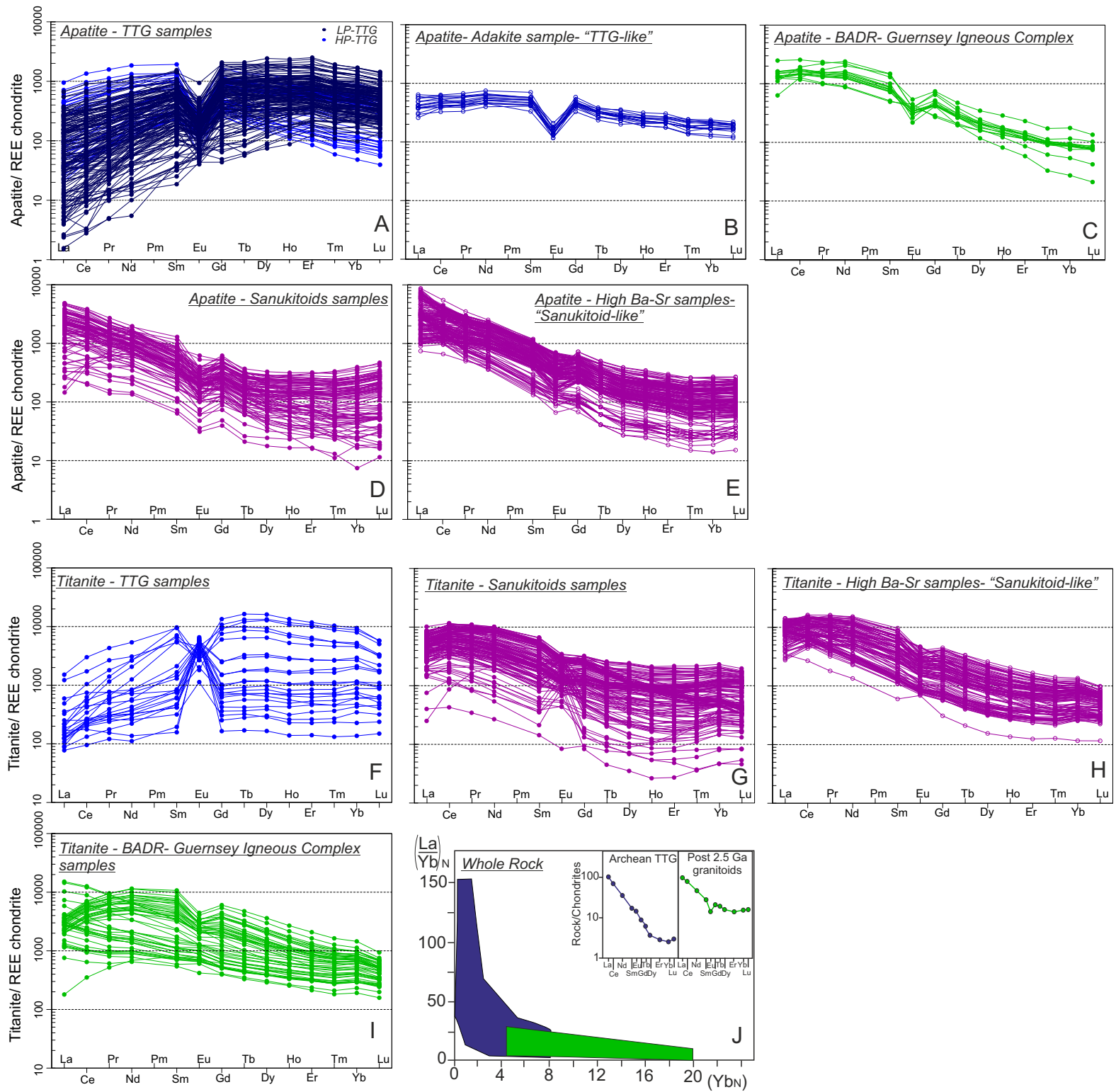


Figure 2 Bruand et al.

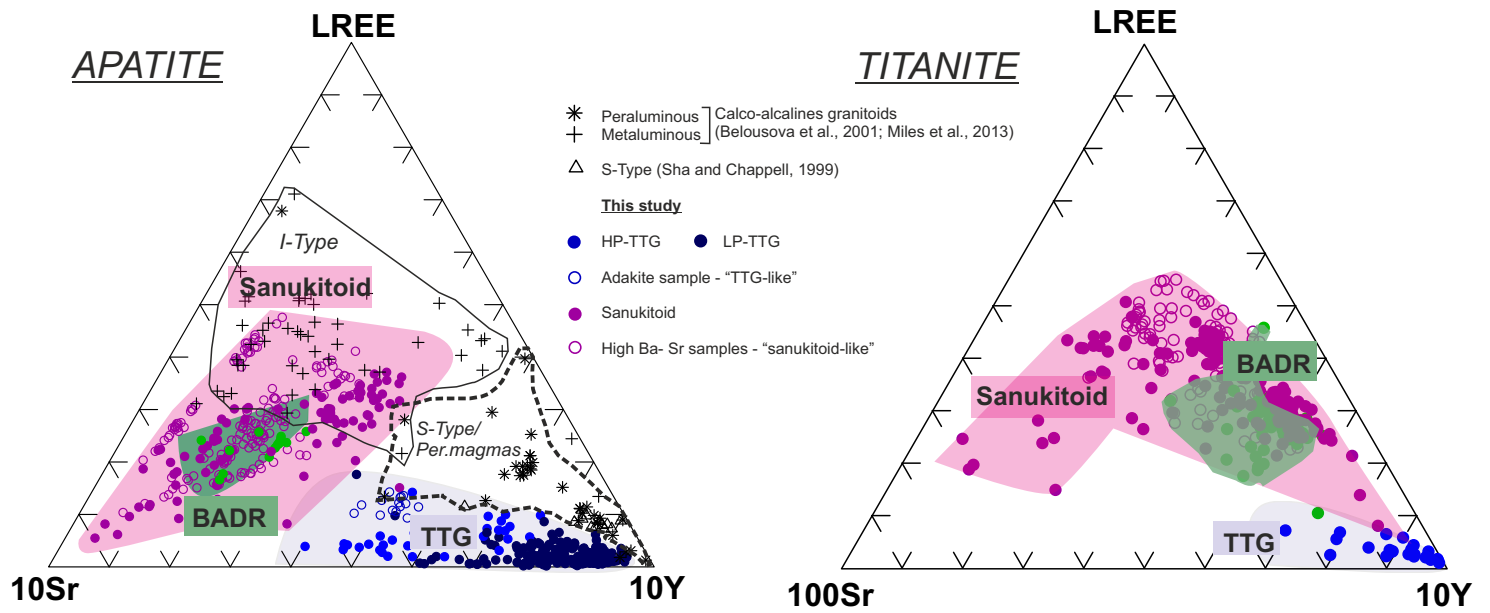
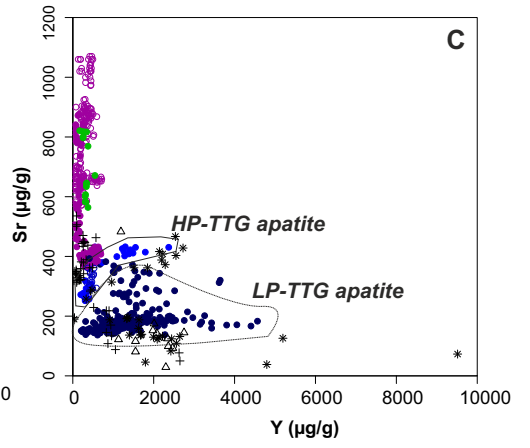
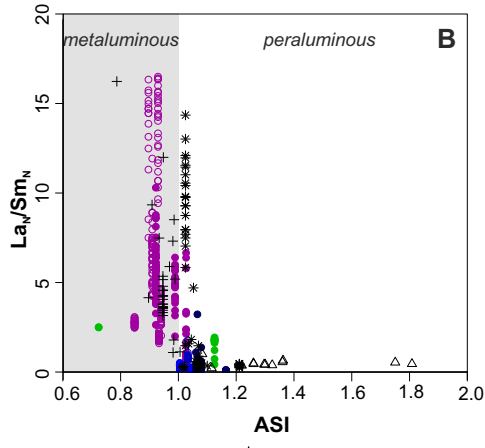
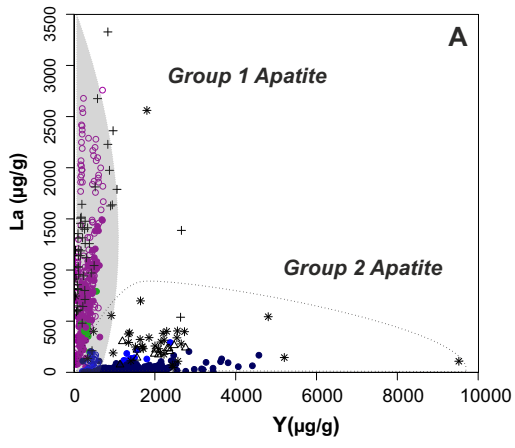


Fig. 3



This study: ● HP-TTG ● LP-TTG ● Sanukitoids ○ Adakite sample "TTG-like" ○ High Ba- Sr samples "sanukitoid-like" \* Peraluminous + Metaluminous  
 ] Calc-alkaline granitoids (Belousova et al., 2001; Miles et al., 2013) △ S-Type (Sha and Chappell, 1999)

## Accessory mineral constraints on crustal evolution: elemental fingerprints for magma

E. Bruand, M. Fowler, C. Storey, O. Laurent, C. Antoine, M. Guitreau,  
E. Heilimo, O. Nebel

### Supplementary Information

#### *Sample description*

In this work, we have systematically analysed apatite and titanite (when present) from a range of granitoids from the Archean toward the Phanerozoic (Fig. 1).

#### **TTG and TTG-like**

TTG are the main components of Archean cratons and have been interpreted as the results of melted garnet-bearing metabasalt either in subduction or intraplate contexts. They are silica –rich ( $\text{SiO}_2 > 64$  wt%), have a high  $\text{Na}_2\text{O}$  content (3-7 wt%), are low in ferromagnesian, Cr and Ni contents (Moyen and Martin 2012 and references therein). In this contribution, TTG from different cratons have been studied : Kaapvaal craton (South Africa), Karelia craton (Finland) and the Slave province (Acasta, Canada). In the Kaapvaal craton, the TTG sampled (DWK-04 and HRG-1) are from the Pietersburg block and have been both dated at about 2.9 Ga (Laurent et al. 2013). Karelia's samples (EPHE 2004-369.2 and 413.1) have also been characterised (Mikkola et al. 2011) and have been dated at about 2.8 Ga. Acasta samples (AG09-009/14/15 and 16) have previously been characterised for their whole rocks and are dated between 3.9 Ga (AG09-016) and 3.6 Ga (AG09-009/14/15; Guitreau et al. 2014; Mojzsis et al. 2014). For comparison with those TTG, a TTG-like sample was also analysed. It is an early permian biotite microgranite from Marie Byrd Land

(Antarctica). This sample exposes the same whole rock characteristics as the TTG (high  $\text{SiO}_2$ , sodic nature, low  $\text{K}_2\text{O}/\text{Na}_2\text{O} < 0.5$ , High Sr  $> 400$  and La, low Y; Pankrust et al. 1998) and is therefore belonging to the high-silica adakites group previously defined by Martin et al. (2005). Their main petrographic characteristics are compiled in Table A.1. All samples have apatite and zircon as accessory phases. One sample has titanite (EPHE 2004- 369.2) and sample AG09 009 has small grains of primary monazite surrounded by secondary allanite, apatite and grains of thorite (Antoine et al., personal communication). All Acasta's samples have clusters of secondary fibrous allanite.

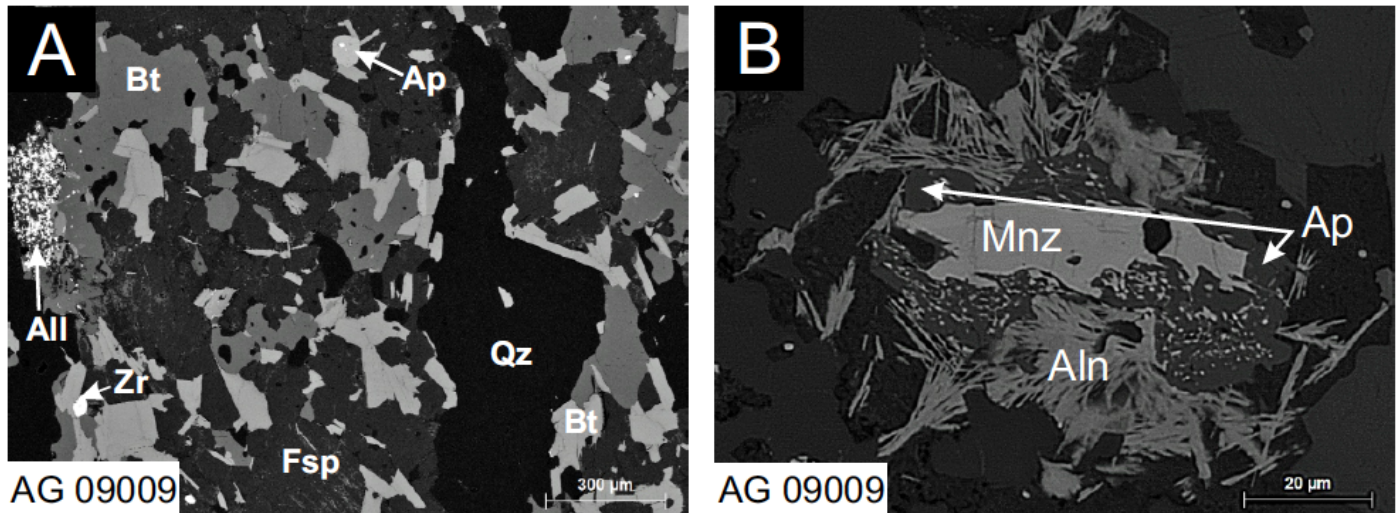


**Fig. 1- BSE images of TTG (Acasta) with aggregates of secondary fibrous allanite. Careful study of the samples allowed to find preserved primary monazite partly replaced by secondary allanite, apatite and thorite due to later metamorphic overprinting (Antoine et al., personal communication).**

## Sanukitoids and High Ba-Sr granite

Sanukitoids are typical magmas appearing at the Archean-Proterozoic transition. Their chemistries have been interpreted as the result of the interaction between a melt or fluid and a mantle wedge. They are chemically characterised by silica contents up to 60 wt%, Cr  $> 100$  ppm, high  $\text{Na}_2\text{O}$ ,  $\text{K}_2\text{O}$ , Sr, Ba and LREE contents (Martin et al. 2005).

Sanukitoids samples in this study are from the Karelia and Kaapvaal cratons. Sanukitoids from Kaapvaal are a granodiorite and a diorite from the Limpopo belt (MAT 43 and MAT 13, (Laurent et al. 2014a, b, 2017; Laurent and Zeh 2015) and have been dated around 2.7 Ga. Karelia's samples have also been dated around 2.7 Ga (Heilimo et al. 2011) and are both granodioritic in composition.

The high Ba-Sr suite studied here are the modern equivalent of the sanukitoids (Fowler and Rollinson 2012). They are Caledonian granitoids that have been characterised for major, trace, Nd and O isotopes whole rock composition (Fowler et al. 2001; Fowler et al. 2008). The whole-rock chemistry of the selected samples range from granodiorite to granitic compositions. They are located in the northwestern part of Scotland and have been dated at about 425 Ma (Kocks et al. 2014). Description of their mineralogy can be found in Bruand et al. (2014). All samples contain apatite,

titanite and zircon with some containing allanite or monazite. Trace elements data on accessory phases available in this contribution are from Bruand et al. (2014).

## Basalt-Andesite-Dacite-Rhyolite (BADR)

The « modern » granitoids samples (BADR samples) studied in this contribution are from the Guernsey igneous complex (Channel Island) which is part of the Armorican massif and is divided geologically into two main parts. The southern part mainly comprises Paleoproterozoic gneisses (The Icartian gneisses; Samson et al. 2003) intruded by syntectonic and subsequently deformed Neoproterozoic granitoids (Perelle quartz-diorite and l'Erée granite; Samson and D'Lemos 1999) and the northern part is dominated by the undeformed, Neoproterozoic Northern Igneous Complex. In order to cover the entire Neoproterozoic plutonic history, samples studied here are from deformed (11-EG-07) and undeformed granitoids (11-BD-02). Sample 11-BD-02 is a diorite while 11-EG-07 is a granodiorite (Appendix A.1). Plutonic rocks from the Northern Igneous Complex have a calc-alkaline signature and were emplaced at the end of the Cadomian orogeny (c.a. 560-550 Ma, de Bremond d'Ars et al. 1992). They are referred to by Brown et al. (1990) as post-tectonic units. The deformed sample from l'Erée granite (EG-07) in the southern part of the island and its field relationships (e.g. the presence of dykes absent in the north and the presence of foliation) indicate that it belongs to the early Cadomian event and intruded the Icartian basement syntectonically. This is also suggested by age data (Samson et al. 2003) at 614 Ma +/- 2 Ma. The early Cadomian intrusions in the Channel Islands are calc-alkaline in composition and have typical volcanic arc granites signature (Power et al. 1990). Description of main phases can be found in table 1. Accessory phases found in the Guernsey igneous complex are apatite, zircon and +/- titanite.

**Table S-1. Samples description**

		Type	Age (Ma)	literature	Comments	Accessories
<b>Kaapvaal craton, South Africa</b>	DWK-04	TTG	2941	Laurent et al., 2013; Laurent et al, 2014 WR	Trondhjemite	apatite, zircon
	HRG-1	TTG	2933		Trondhjemite	apatite zircon
	MAT 13	Sanukitoid	2679	Laurent et al., 2013; Laurent et al, 2014 WR	Granodiorite	apatite, titanite, zircon
<b>Karelia craton, Finland</b>	EPHE 2004 369.2	TTG	2821	Mikkola et al., 2011 corresponding sample A1857	Granodiorite	apatite, titanite, zircon, aln
	EPHE 2013 413.1	TTG	2785	Käpyaho et al., 2006 corresponding sample A1705	Tonalite	apatite, zircon
	STHA-2009-316	Sanukitoid	2722	Heilimo et al., 2011 corresponding sample A1339	Granodiorite	apatite, titanite, zircon
	A572	Sanukitoid	2723	Heilimo et al., 2011	Granodiorite	apatite, titanite, zircon
<b>Marie Byrd Land, Antarctica</b>	402-1D	Adakite	early permian	Pankhrust et al., 1998	Biotite microgranite	apatite, zircon
<b>High Ba-Sr, Scotland</b>	SR1	Sanukitoid-like	425	Fowler et al. 2008; Fowler and Rollinson, 2012	Granodiorite	apatite, titanite, zircon
	SR2	Sanukitoid-like	425		Appinite	apatite, titanite, zircon
	SR3	Sanukitoid-like	425		Granodiorite	apatite, titanite, zircon, aln
	SR4	Sanukitoid-like	425		Granodiorite	apatite, titanite, zircon
	RA1	Sanukitoid-like	425	Kocks et al., 2014; Fowler et al. 2001, 2008; Fowler and Rollinson, 2012	Appinite	apatite, titanite, zircon
	RT1	Sanukitoid-like	425		Tonalite	apatite, titanite, zircon, aln
	R2	Sanukitoid-like	425		Tonalite	apatite, titanite, zircon, aln
	RGH1	Sanukitoid-like	425		Granite	apatite, titanite, zircon
<b>Slave Province, Acasta, Canada</b>	AG09 009	TTG	3600	Mojzsis et al 2014 for WR and Guitreau et al. 2012 for dating	Granitic orthogneiss	apatite, zircon, monazite
	AG09 014	TTG	3600		Tonalitic orthogneiss	apatite, zircon
	AG09 015	TTG	3600		Tonalitic orthogneiss	apatite, zircon
	AG09 016	TTG	3947		Tonalitic orthogneiss	apatite, zircon
<b>Guernsey Igneous Province, Channel Islands</b>	11-BD-02	Arc Magma- Diorite	560-550		Bordeaux diorite locality	apatite, titanite, zircon
	11-EG-07	Arc Magma - Granite	614	Samson et al. (2014)	L'Erée granite locality/granodiorite	apatite, titanite, zircon

Sample	GPS Coordinates	Sample	GPS Coordinates	Sample	GPS Coordinates
DWK-04 <sup>1</sup>	Lat 23.611944S Long 30.328889E	AG09016 <sup>3</sup>	Lat 65.160650N Long 115.546033W	SR4 <sup>6</sup>	Lat 56.730766N Long 5.540805W
HRG-1 <sup>1</sup>	Lat 23.792512S Long 29.127496E	402.1D <sup>4</sup>	Pankhrust et al. 1998	SR3 <sup>6</sup>	Lat 56.685100N Long 5.627994W
EPHE 2004 369.2 <sup>2</sup>	Lat 65.27511096N Long 29.18714509E	STHA-2009-316 <sup>5</sup>	Lat 63.22764732N Long 30.65472253E	SR1 <sup>6</sup>	Lat 56.689443N Long 5.602272W
EPHE 2013-413.1 <sup>2</sup>	Lat 64.1841557N Long 28.874444 E	A572 <sup>5</sup>	Lat 64.44985108N Long 29.00994815E	RT1 <sup>6</sup>	Lat 57.993611N Long 4.197395W
AG09009 <sup>3</sup>	Lat 65.170217N Long 115.562683W	MAT-13 <sup>1</sup>	Lat 23.525368S Long 29.703366E	11-EG-07*	Lat 49.454750N Long 2.655250W
AG09014 <sup>3</sup>	Lat 65.160250N Long 115.547317W	RHG-1 <sup>6</sup>	Lat 58.010645N Long 4.250916W	11-BD-02*	Lat 49.490000N Long 2.578361W
AG09015 <sup>3</sup>	Lat 65.160250N Long 115.547317W	R2 <sup>6</sup>	Lat 57.996508N Long 4.185728W		

## *Analytical techniques*

The samples were crushed (jaw-crusher, ball mill or Selfrag™), sieved (<355 µm, 355-500 µm and 500-1000 µm fractions) and passed over a Wilfley table. A diamagnetic separator was then used to obtain fractions of different heavy minerals based on their diamagnetic properties. Titanite and apatite were handpicked, mounted in epoxy resin discs and polished for in-situ chemical analysis. Titanite and apatite have also been analysed within thick sections (c.150µm).

## **Image acquisition**

Back-scattered electron (BSE) images of titanite were taken with a scanning electron microscope (SEM) JEOL JSM-6100 at the University of Portsmouth (accelerating voltage = 20 kV). Cathodoluminescence (CL) images of apatite

were taken with a KeDev Centaurus cathodoluminescence detector housed within a JEOL 6060LV SEM at the University of Portsmouth, or a JEOL JSM-5910 LV with an OPEA detector at the Laboratoire Magmas et Volcans (Clermont-Ferrand, France; accelerating voltage = 15 kV).

## Electron probe microanalysis (EPMA)

A Cameca SX-100 microprobe at Bristol University was used for determination of major elements in titanite and zircon using TAP, LPET, PET and LLIF crystals. PC0, TAP, LPET and LLIF crystals were used for apatite. An electron beam of 1  $\mu\text{m}$  was used for titanite and 10  $\mu\text{m}$  for apatite, both with 20 kV accelerating voltage and, 40 nA and 10 nA beam currents respectively. An electron beam of 5  $\mu\text{m}$  was used for zircon with an accelerating voltage of 17 kV and a beam current of 100 nA. Several trace elements in these minerals were also analysed for comparison with laser ablation ICP-MS (LA-ICPMS) data. The Durango apatite standard (Marks *et al.*, 2012) and the 91500 zircon standard (Wiedenbeck *et al.*, 2004) were analysed during sessions to monitor data quality.

## Trace element analysis : LA-ICPMS

Trace element contents of titanite and apatite were determined by LA-ICPMS at the University of Portsmouth using an Agilent 7500cs (quadrupole) ICPMS and a New-Wave UP213 ( $\lambda=213$  nm) solid state Nd:YAG laser, or at the Laboratoire Magmas et Volcans (Clermont-Ferrand, France) using an Element XR associated with an excimer laser ATL (Resonetics M-50E;  $\lambda=193$  nm). Each analysis consisted of ca. 30 s background acquisition and 60 to 80 s sample acquisition. The diameter of the laser beam was 30  $\mu\text{m}$  for titanite and 9-30  $\mu\text{m}$  for apatite.

Internal references used for normalisation of LA-ICPMS data were  $^{43}\text{Ca}$  for apatite and titanite and were obtained by EPMA. Details of instruments conditions can be found in Table S-2. Geochemical Data Toolkit (GCDkit, Version 5.0; Janousek *et al.* 2006) was used to plot the data. **All data trace elements on accessory phases and whole rock data presented in this contribution can be found as a supplementary file (Table S.3).**

**Table S-2 – Laser models and conditions to measure apatite and titanite trace elements**

	Frequency	Fluence	Laser Spot	External Standard	Secondary standard analysed during runs
<b>Excimer laser ATL 193 nm Resonetics M-50E with XR Element (Laboratoire Magmas et Volcans)</b>	1-2 Hz	2.8-2.9 J/cm <sup>2</sup>	9-12 $\mu\text{m}$	NIST 610 (Pearce <i>et al.</i> , 1997) or GSE-1G (Jochum <i>et al.</i> 2005)	Durango for Apatite (Marks <i>et al.</i> , 2013)
<b>New-Wave UP213 (<math>\lambda=213</math> nm) solid state Nd:YAG laser and 7500 cs Agilent (University of Portsmouth)</b>	10 Hz	4 J/cm <sup>2</sup>	30 $\mu\text{m}$	NIST 610	Durango for Apatite (Marks <i>et al.</i> , 2013) and in house Khan standard for titanite
<b>Excimer laser S155 Resonetics</b>	5 Hz	3-4 J/cm <sup>2</sup>	29 $\mu\text{m}$	NIST 610	Durango

with Element 2 (Goethe  
Universitaet Frankfurt)

*Table S-3 – Whole rock analysis and trace elements analysis on apatite and titanite from the different samples studied in this contribution. Chondrite values used for normalization are from Boynton (1984).*

### ***Supplementary Information References***

- Boynton W V (1984) Chapter 3 - Cosmochemistry of the Rare Earth Elements: Meteorite Studies. In: Henderson P (ed) Rare Earth Element Geochemistry. Elsevier, pp 63–114
- Brown M, Power GM, Topley CG, D’Lemos RS (1990) Cadomian magmatism in the North Armorican Massif. *Geol Soc London, Spec Publ* 51:181–213. doi: 10.1144/GSL.SP.1990.051.01.12
- Bruand E, Storey C, Fowler M (2014) Accessory mineral chemistry of high Ba-Sr granites from Northern Scotland: Constraints on petrogenesis and records of whole-rock Signature. *J Petrol.* doi: 10.1093/petrology/egu037
- de Bremond d’Ars J, Martin H, Auvray B, Lécuyer C (1992) Petrology of a magma chamber: the Plutonic Complex of Guernsey (Channel Islands, UK). *J Geol Soc London* 149:701–708. doi: 10.1144/gsjgs.150.4.0788
- Fowler M, Rollinson H (2012) Phanerozoic sanukitoids from Caledonian Scotland: Implications for Archean subduction. *Geology* 40:1079–1082. doi: 10.1130/G33371.1
- FOWLER MB, HENNEY PJ, DARBYSHIRE DPF, GREENWOOD PB (2001) Petrogenesis of high Ba-Sr granites: the Rogart pluton, Sutherland. *J Geol Soc London* 158:521–534. doi: 10.1144/jgs.158.3.521
- Fowler MB, Kocks H, Darbyshire DPF, Greenwood PB (2008) Petrogenesis of high Ba-Sr plutons from the Northern Highlands Terrane of the British Caledonian Province. *Lithos* 105:129–148. doi: 10.1016/j.lithos.2008.03.003
- Guitreau M, Blichert-Toft J, Mojzsis SJ, et al (2014) Lu-Hf isotope systematics of the Hadean-Eoarchean Acasta Gneiss Complex (Northwest Territories, Canada). *Geochim Cosmochim Acta* 135:251–269. doi: 10.1016/j.gca.2014.03.039
- Heilimo E, Halla J, Huhma H (2011) Single-grain zircon U-Pb age constraints of the western and eastern sanukitoid zones in the Finnish part of the Karelian Province. *Lithos* 121:87–99. doi: 10.1016/j.lithos.2010.10.006
- Janousek V, Farrow CM, Erban V (2006) Interpretation of Whole-rock Geochemical Data in Igneous Geochemistry : Introducing Geochemical Data Toolkit ( GCDkit ). 47:1255–1259. doi: 10.1093/petrology/egl013
- KOCKS H, STRACHAN R, EVANS J, FOWLER M (2014) Contrasting magma emplacement mechanisms within the Rogart igneous complex, NW Scotland, record the switch from regional contraction to strike-slip during the Caledonian orogeny. , 151(5), . *Geol Mag* 151:899–915.
- Laurent O, Martin H, Moyen JF, Doucelance R (2014a) The diversity and evolution of late-Archean granitoids: Evidence for the onset of “modern-style” plate tectonics between 3.0 and 2.5 Ga. *Lithos* 205:208–235. doi: 10.1016/j.lithos.2014.06.012
- Laurent O, Paquette J, Martin H, Doucelance R (2013) LA-ICP-MS dating of zircons from Meso- and Neoproterozoic granitoids of the Pietersburg block ( South Africa ): Crustal evolution at the northern margin of the Kaapvaal

- craton. *Precambrian Res* 230:209–226. doi: 10.1016/j.precamres.2013.02.009
- Laurent O, Rapopo M, Stevens G, et al (2014b) Contrasting petrogenesis of Mg–K and Fe–K granitoids and implications for post-collisional magmatism: Case study from the Late-Archean Matok pluton (Pietersburg block, South Africa). *LITHOS* 196–197:131–149. doi: 10.1016/j.lithos.2014.03.006
- Laurent O, Zeh A (2015) A linear Hf isotope-age array despite different granitoid sources and complex Archean geodynamics: Example from the Pietersburg block (South Africa). *Earth Planet Sci Lett* 430:326–338. doi: 10.1016/j.epsl.2015.08.028
- Laurent O, Zeh A, Gerdes A, Villaros A (2017) How do granitoid magmas mix with each other? Insights from textures, trace element and Sr – Nd isotopic composition of apatite and titanite from the Matok pluton (South Africa). doi: 10.1007/s00410-017-1398-1
- Martin H, Smithies RH, Rapp R, et al (2005) An overview of adakite, tonalite-trondhjemite-granodiorite (TTG), and sanukitoid: Relationships and some implications for crustal evolution. *Lithos* 79:1–24. doi: 10.1016/j.lithos.2004.04.048
- Mikkola P, Huhma H, Heilimo E, Whitehouse M (2011) Archean crustal evolution of the Suomussalmi district as part of the Kianta Complex, Karelia: Constraints from geochemistry and isotopes of granitoids. *Lithos* 125:287–307. doi: 10.1016/j.lithos.2011.02.012
- Mojzsis SJ, Cates NL, Caro G, et al (2014) Component geochronology in the polyphase ca. 3920Ma Acasta Gneiss. *Geochim Cosmochim Acta* 133:68–96. doi: 10.1016/j.gca.2014.02.019
- Moyen J, Martin H (2012) Lithos Forty years of TTG research. *LITHOS* 148:312–336. doi: 10.1016/j.lithos.2012.06.010
- Pankrust RJ, Weaver SD, Bradshaw JD, et al (1998) Geochronology and geochemistry of pre-Jurassic superterranes in Marie Byrd Land, Antarctica. *J Geophys Res* 103:2529–2547.
- Power GM, Brewer TS, Brown M, Gibbons W (1990) Late Precambrian foliated plutonic complexes of the Channel Islands and La Hague: early Cadomian plutonism. *Geol Soc London, Spec Publ* 51:215–229. doi: 10.1144/GSL.SP.1990.051.01.13
- Samson SD, D’Lemos RS (1999) A precise late Neoproterozoic U-Pb zircon age for the syntectonic Perelle quartz diorite, Guernsey, Channel Islands, UK. *J Geol Soc London* 156: 1:47–54. doi: 10.1144/gsjgs.156.1.0047
- Samson SD, D’Lemos RS, Blichert-Toft J, Vervoort J (2003) U-Pb geochronology and Hf-Nd isotope compositions of the oldest Neoproterozoic crust within the Cadomian orogen: New evidence for a unique juvenile terrane. *Earth Planet Sci Lett* 208:165–180. doi: 10.1016/S0012-821X(03)00045-1